frontiers | Frontiers in Climate

TYPE Original Research
PUBLISHED 03 December 2025
DOI 10.3389/fclim.2025.1688860

OPEN ACCESS

EDITED BY
Yaoping Wang,
The University of Tennessee, Knoxville, United States

REVIEWED BY
Yali Zhu,
Chinese Academy of Sciences (CAS), China
Shunwu Zhou,
Nanjing University of Information Science and Technology, China

*CORRESPONDENCE
Chao Luo
✉ luochao001@126.com

RECEIVED 19 August 2025
REVISED 04 November 2025
ACCEPTED 17 November 2025
PUBLISHED 03 December 2025

CITATION
Shi H, Long Y, Luo C, Wu S, Wang Z, Guo W and Wu J (2025) Attribution of contrasting warm-season convective boundary layer height trends over the Tianshan-Taklamakan-Oasis region to thermodynamic and moisture drivers. *Front. Clim.* 7:1688860. doi: 10.3389/fclim.2025.1688860

Attribution of contrasting warm-season convective boundary layer height trends over the Tianshan-Taklamakan-Oasis region to thermodynamic and moisture drivers

Han Shi[1,2], Yanfei Long[1], Chao Luo[1]*, Sijiang Wu[1], Zhengbo Wang[1], Wenbei Guo[1,3] and Jianxun Wu[1]

[1]Northwest Institute of Nuclear Technology, Xi'an, China, [2]Computer Science of Technology, Zhejiang University, Hangzhou, China, [3]College of Meteorology and Oceanography, National University of Defense Technology, Changsha, China

The convective boundary layer height (CBLH) plays a crucial role in regulating atmospheric mixing and land-atmosphere interactions, yet its spatiotemporal variability in the arid, topographically complex Xinjiang region of northwestern China remains insufficiently understood. Using ERA5-Land reanalysis (1985–2024 for CBLH; 2000–2024 for driving factors) and GLASS LAI data for April–September, CBLH characteristics and trends were investigated through the Mann–Kendall test, Theil–Sen slope estimation, multiple linear regression (MLR), and principal component analysis (PCA). Results show that the Tarim and Junggar Basins exhibit higher CBLH than the surrounding mountains, with seasonal peaks in June–July. From 2000 to 2024, a significant CBLH increase occurred in the Tianshan Mountains during July, while a marked decline was observed over the Taklamakan Desert in August. MLR results indicate that August CBLH over the Taklamakan is enhanced by strong surface heating but constrained by the cooling and moistening effects of nearby oases. In contrast, July CBLH over the Tianshan is amplified by local heating and winds, yet suppressed by both local and remote moisture inputs and sensible heat flux anomalies. PCA further supports these findings, linking the Tianshan's July increases to reduced net longwave cooling, stronger sensible heating, and lower atmospheric pressure, and the Taklamakan's August decreases to enhanced cooling, weakened heating, and increased humidity. These results highlight the region's divergent CBLH responses to local forcing and cross-regional interactions, emphasizing that both warming-induced increases and moisture-driven declines must be considered in future regional climate assessments.

KEYWORDS

convective boundary layer height, multiple linear regression, principal component analysis, Tianshan Mountains, thermodynamic forcing, moisture advection, cross-regional influence

1 Introduction

The atmospheric boundary layer (ABL)—the lowest part of the troposphere—is a highly dynamic zone dominated by turbulence and strongly influenced by the properties of the underlying surface. It adjusts to surface forcing within timeframes of less than an hour (Stull, 1988). The depth of the ABL reflects the capacity of the atmosphere to hold and redistribute heat, moisture, and other scalars, thereby mediating the vertical exchange of energy, momentum, and chemical species between the surface and the free atmosphere (Salam et al., 2024; Wang and Zhang, 2022). Within the ABL, different regimes can develop depending on the prevailing surface energy balance and atmospheric stability. One of the most prominent is the convective boundary layer (CBL), which forms under strong surface heating and unstable stratification, and is characterized by vigorous turbulence and efficient vertical mixing. Convective boundary layer height (CBLH) serves as a sensitive indicator of atmospheric mixing processes, with documented impacts on air quality, cloud development, precipitation formation, and climate feedback mechanisms (Zhang et al., 2022; Brunsell et al., 2011).

Projected climate change is expected to modify land-atmosphere interactions and the dynamics of the boundary layer, particularly in arid and semi-arid climates (He et al., 2024). Mid-latitude mountain regions are especially vulnerable in this context, as complex topography enhances spatial gradients in surface forcing and compels distinct atmospheric responses (Zardi, 2007; Lieman and Alpert, 1993). Examining CBLH behavior in such environments is therefore critical for understanding local manifestations of large-scale warming.

Located in northwestern China, Xinjiang offers a striking example of topographic complexity: the Altai Mountains in the north, the Tianshan Mountains across the interior, and the Kunlun Mountains in the south enclose the Junggar and Tarim Basins to form the well-known "three mountains flanked by two basins" configuration. As illustrated in Figure 1, the terrain is further subdivided here into three characteristic subregions: the Tianshan Mountains, the oasis belt along the southern foothills of the Tianshan, and the Taklamakan Desert (this subdivision is adopted because the Tianshan and the Taklamakan Desert exhibit distinct and representative CBLH changes that warrant focused investigation, while the oasis belt serves as a transitional zone whose influence on both regions also merits consideration). These pronounced elevation contrasts shape patterns of temperature, soil moisture, and aerodynamic roughness, which in turn influence CBL development through mesoscale circulations (He et al., 2020; Wang et al., 2023). The region's arid climate—with strong solar forcing, marked diurnal temperature ranges, and low evapotranspiration—commonly produces a deep CBL during the warm season (April–September) (Li et al., 2023; Salam et al., 2024; Wang and Zhang, 2022), making Xinjiang a valuable natural laboratory for boundary layer studies.

Earlier investigations have shown that warm-season CBLHs over Central Asia's arid zones are often higher than those in more humid counterparts at similar latitudes (Wang et al., 2023, 2021; Man et al., 2021), largely owing to intense sensible heating. Yet, research to date has tended to concentrate on specific localities—such as the Tarim Basin or sections of the Junggar Basin—rather than analyzing Xinjiang as an integrated whole, with its mountain ranges and intervening basins considered together. Moreover, there has been limited systematic exploration of CBLH variability on seasonal to interannual timescales. Studies assessing its controlling factors often depend on grid-to-grid correlation methods applied to reanalysis or model grids (Wu et al., 2024), which can obscure the role of coherent large-scale circulation features. Such gaps constrain our understanding of the processes driving CBLH evolution in this distinctive terrain. Although the oasis belt is recognized as a transitional climatic zone with potential modulatory effects—such as cold-island cooling and enhanced moisture advection—it is not analyzed in isolation for trend statistics due to the absence of significant changes in warm-season CBLH (see Section 4). Instead, its role is assessed through cross-regional diagnostics, highlighting its influence on adjacent desert and mountain convection.

Beyond local heating effects, Xinjiang's boundary layer dynamics are shaped by its position at the confluence of the mid-latitude westerlies, the Asian monsoon, and regionally generated circulations such as mountain-valley winds (Zhang et al., 2020; Lu et al., 2025). Anticipated reductions in snow and glacier cover, along with changes in surface albedo, are likely to affect these processes (Bhattacharya et al., 2021), with knock-on effects on CBLH characteristics.

Against this backdrop, the present work undertakes a comprehensive evaluation of warm-season (April–September) CBLH across the whole of Xinjiang, explicitly including the Tianshan Mountains and the two major basins. By combining high-resolution reanalysis datasets with diagnostic approaches that incorporate large-scale circulation effects, this study addresses several limitations present in earlier analyses. The resulting insights are intended to inform not only regional weather and climate prediction but also broader assessments of environmental change in complex, climate-sensitive mountain-basin systems.

The principal contributions of this research are as follows:

1. Comprehensive spatiotemporal assessment: it provides the first full-region analysis of warm-season CBLH in Xinjiang, resolving both spatial patterns and temporal variability from seasonal to interannual scales.
2. Mechanism-oriented regional classification: based on spatial variability patterns, Xinjiang is divided into desert, oasis, and Tianshan subregions, with regionally averaged diagnostics clarifying the dominant mechanisms controlling CBLH.
3. Actionable scientific insights: it establishes robust conclusions on spatial organization and driving factors of CBLH variability, with direct implications for boundary layer processes, land-atmosphere coupling, and climate change impacts in arid mountainous environments.

2 Materials and methods

2.1 Data

This study employs two main datasets: the ERA5-Land reanalysis from the European Center for Medium-Range Weather

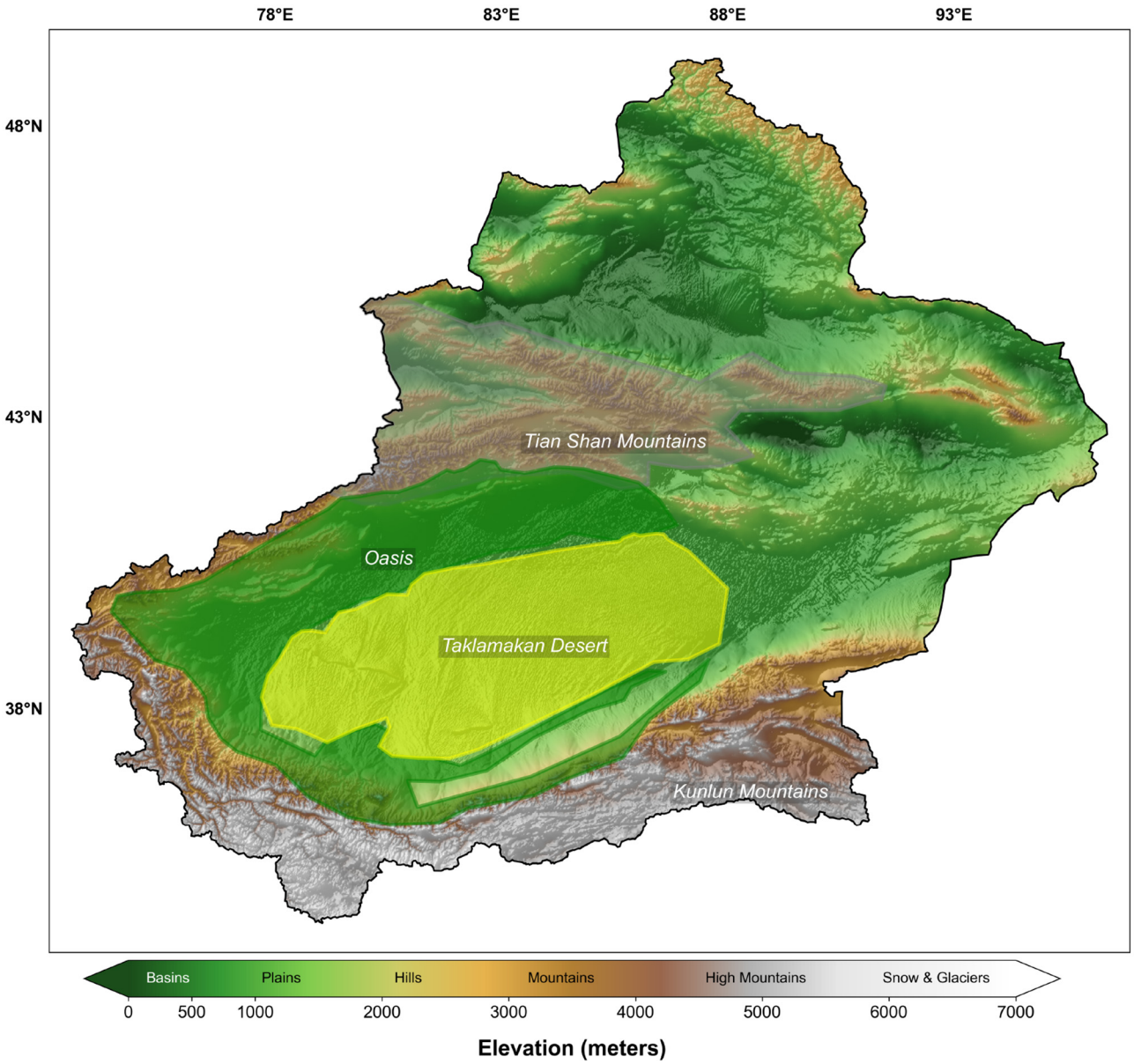

FIGURE 1
Topography of Xinjiang, highlighting the Tianshan Mountains, Oasis, and Taklamakan Desert. The map illustrates the region's major physiographic divisions within the "three mountains flanked by two basins" configuration.

Forecasts (ECMWF) and the Global Land Surface Satellite (GLASS) Leaf Area Index (LAI) product. ERA5-Land provides multiple surface and near-surface meteorological variables with a spatial resolution of 0.25° × 0.25° and hourly resolution (Hersbach et al., 2020; Muñoz Sabater et al., 2021). For this work, data during the warm season (April–September) were used and were selected daily values at 19:00 Beijing Time (11:00 UTC), corresponding to the mature stage of daytime convective development over Xinjiang.

The choice of 19:00 Beijing Time aligns with the mature stage of daytime convective boundary layer development in arid regions like Xinjiang, where CBLH typically reaches its daily maximum in the mid-to-late afternoon (approximately 17:00–19:00 local solar time, as shown in Figure 2), driven by peak sensible heat flux and sustained convection. To further verify this, hourly boundary layer height data from April to September 2023—within a representative area of the Taklamakan Desert (39–40°N, 83–84°E)—were selected. The average values across all grid points for each hour were calculated. 19:00 BT was chosen as it corresponds to the time of most fully developed and mature convection, ensuring the analysis captures the representative maximum CBLH.

The convective boundary layer height (CBLH) record spans 1985–2024, whereas other ERA5-Land variables are available from 2000 to 2024. An exception is runoff, which is provided monthly at 0.1° × 0.1° resolution. The longer CBLH dataset (1985–2024) was utilized to explore the spatiotemporal variations of CBLH in Xinjiang across different time scales, after which the period from

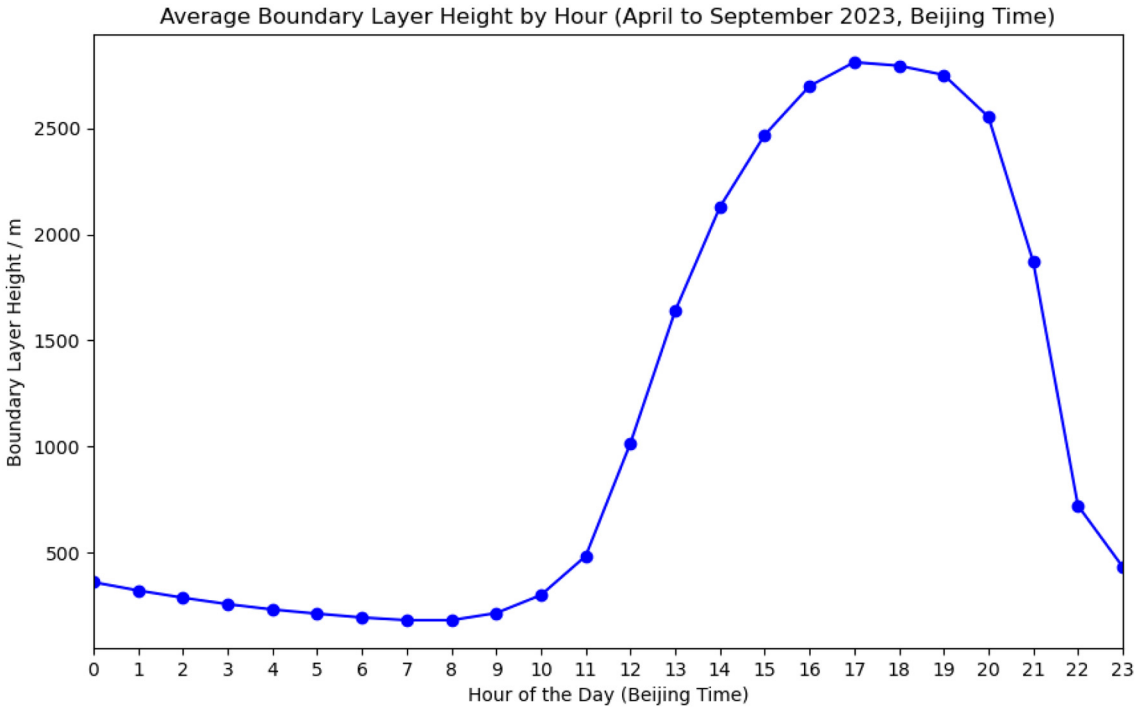

FIGURE 2
Hourly average boundary layer height over a representative area of the Taklamakan Desert (39–40°N, 83–84°E) during April–September 2023 (Beijing Time).

2000 to 2024 was selected for focused analysis; consequently, the driving factors data encompass only 2000–2024.

The LAI dataset used in this study was obtained from the GLASS Version 6 product (Ma and Liang, 2022; Xiao et al., 2016), derived from MODIS observations using a bidirectional long short-term memory (Bi-LSTM) deep learning algorithm. The selected product provides global coverage at a spatial resolution of 0.25° × 0.25° and a monthly frequency from 2000 to 2024, and it has been validated against *in-situ* measurements, exhibiting improved temporal continuity and accuracy compared to standard MODIS LAI products. A summary of all variables, their abbreviations, temporal and spatial resolutions, and time spans is provided in Table 1.

2.2 Methods

2.2.1 Mann–Kendall (MK) trend test

The non-parametric Mann-Kendall (MK) test is employed to detect monotonic trends in long-term time series (Mann, 1945; Kendall, 1975). Given a series $x_1, x_2, \ldots, x_n$, the test statistic S is calculated as:

$$S = \sum_{i=1}^{n-1} \sum_{j=i+1}^{n} \mathrm{sgn}(x_j - x_i) \tag{1}$$

where $\mathrm{sgn}(\cdot)$ is the sign function. The variance of S accounts for ties, and a standardized test statistic Z is used to evaluate significance.

2.2.2 Theil-Sen slope estimation

The Theil-Sen estimator provides a robust, non-parametric estimate of the trend slope by taking the median of all pairwise slopes (Theil, 1950; Sen, 1968):

$$\beta = \mathrm{median}\left(\frac{x_j - x_i}{j - i}\right), \quad \forall\, j > i \tag{2}$$

It is less sensitive to outliers than ordinary least squares fitting.

2.2.3 Multiple linear regression (MLR)

To investigate the relative contributions of multiple predictors (e.g., surface fluxes, wind, soil moisture) to CBLH, multiple linear regression is applied:

$$y = \beta_0 + \beta_1 X_1 + \beta_2 X_2 + \cdots + \beta_p X_p + \varepsilon \tag{3}$$

where y is CBLH and $X_1, \ldots, X_p$ are predictor variables standardized prior to regression. Model significance is assessed via F-tests.

2.2.4 Principal component analysis (PCA)

PCA is used to identify dominant modes of variability in the multivariate dataset and to reduce dimensionality (Jolliffe, 2002). Given a standardized data matrix $\mathbf{X}$, the covariance matrix $\mathbf{C}$ is computed and its eigenvalues (λ_k) and eigenvectors ($\mathbf{e}_k$) are obtained:

$$\mathbf{C}\mathbf{e}_k = \lambda_k \mathbf{e}_k \tag{4}$$

TABLE 1 Summary of datasets used in this study.

Variable (full name)	Abbreviation	Temporal resolution	Spatial resolution	Time span
10 m U component of wind	u10	Daily at 19:00 BJT	0.25° × 0.25°	2000–2024
10 m V component of wind	v10	Daily at 19:00 BJT	0.25° × 0.25°	2000–2024
Boundary layer height	blh	Daily at 19:00 BJT	0.25° × 0.25°	1985–2024
Runoff	ro	Monthly	0.1° × 0.1°	2000–2024
Skin temperature	skt	Daily at 19:00 BJT	0.25° × 0.25°	2000–2024
Specific humidity	q	Daily at 19:00 BJT	0.25° × 0.25°	2000–2024
Surface latent heat flux	slhf	Daily at 19:00 BJT	0.25° × 0.25°	2000–2024
Surface sensible heat flux	sshf	Daily at 19:00 BJT	0.25° × 0.25°	2000–2024
Surface net solar radiation	ssr	Daily at 19:00 BJT	0.25° × 0.25°	2000–2024
Surface net thermal radiation	str	Daily at 19:00 BJT	0.25° × 0.25°	2000–2024
Surface pressure	sp	Daily at 19:00 BJT	0.25° × 0.25°	2000–2024
Total cloud cover	tcc	Daily at 19:00 BJT	0.25° × 0.25°	2000–2024
Volumetric soil water content (layer 3)	swvl3	Daily at 19:00 BJT	0.25° × 0.25°	2000–2024
Leaf Area Index (GLASS V6)	LAI	Monthly	0.25° × 0.25°	2000–2024

BJT, Beijing time.

The principal components are then:

$$\mathbf{PC}_k = \mathbf{X}\mathbf{e}_k \tag{5}$$

allowing the identification of spatial and temporal patterns in CBLH variability and its drivers.

To ensure reproducibility, all analyses, including MLR and PCA, were implemented using Python. Data processing and statistical computations were performed with the following packages: NumPy for array operations and numerical computations, Pandas for data manipulation and regional averaging, SciPy for statistical tests, and scikit-learn for MLR fitting (via LinearRegression) and PCA implementation (via PCA class). No additional external libraries were installed beyond these standard ones. Prior to MLR and PCA, preprocessing steps included: (1) spatial averaging of meteorological variables over three predefined subregions to capture representative values; this was achieved by delineating regional boundaries based on topographic and land-cover criteria using latitude-longitude grids from ERA5-Land data, then computing arithmetic means across grid cells within each region via Pandas groupby operations on spatially masked DataFrames; (2) temporal filtering to focus on warm-season months (April–September) at 19:00 Beijing Time; and (3) standardization of all predictor variables to have zero mean and unit variance using scikit-learn's StandardScaler, which mitigates multicollinearity in MLR and ensures scale-invariance in PCA. For MLR, stepwise forward selection was applied using custom Python functions to iteratively add predictors based on p-value thresholds (<0.05), with model fitting via scikit-learn's LinearRegression and significance assessed through SciPy's F-test. The final model coefficients and R^2 values were computed post-selection. For PCA, the standardized data matrix was input to scikit-learn's PCA class with default parameters, extracting eigenvalues, eigenvectors, and principal components; explained variance ratios were visualized via scree plots generated with Matplotlib, and correlations between PCs and CBLH were calculated using NumPy's corrcoef function.

3 Results

3.1 Spatial distribution of the maximum CBLH during the warm season over Xinjiang in the past 25 years

Figure 3 presents the spatial distribution of the monthly maximum convective boundary layer height (CBLH) in Xinjiang for each month of the warm season (April–September) during 2000–2024. The CBLH maxima exhibit a clear coupling with regional topography, with consistently higher values over the Tarim Basin and Junggar Basin compared to the surrounding mountain ranges. In June and July, maximum CBLH values in the Tarim Basin approach 4,000 m, while those in the Junggar Basin reach about 3,500 m, both substantially exceeding the values observed in April, May, August, and September. The seasonal peak in June–July coincides with the period of highest solar elevation and strongest solar radiation in the Northern Hemisphere, conditions that favor deep convective boundary layer development. In contrast, the Altai Mountains, Tianshan Mountains, and Kunlun Mountains generally exhibit lower CBLH maxima throughout the warm season.

3.2 Trend analysis of warm-season CBLH in Xinjiang over the past 25 years

Figure 4 shows the spatial distribution of the monthly trends in convective boundary layer height (CBLH) over Xinjiang during the

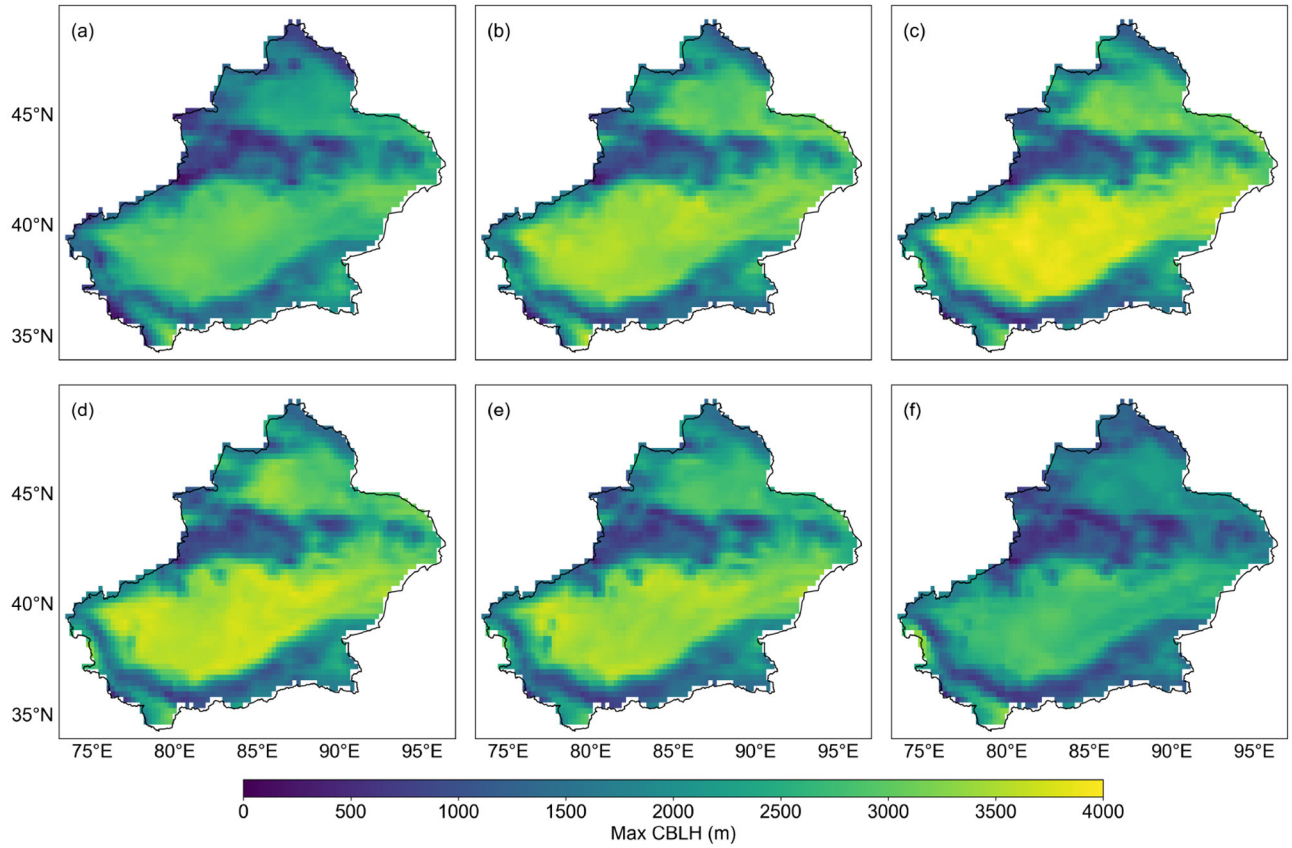

FIGURE 3
Spatial distribution of the monthly maximum convective boundary layer height (CBLH) over Xinjiang during the warm season (April–September) for the period 2000–2024. **(a–f)** Correspond to April, May, June, July, August, and September, respectively.

warm season (April–September) from 2000 to 2024, as quantified by the Sen's slope estimator after the Mann–Kendall significance test. Only statistically significant trends at the $p < 0.05$ level are displayed. The most pronounced positive trends occur in July over the Tianshan Mountains, particularly along the northern slopes, where the increase is both stronger and spatially more extensive than on the southern slopes. June also shows a notable but more spatially limited increase in CBLH over the Tianshan region, whereas trends in the other months are generally weak and insignificant. Conversely, significantly negative CBLH trends are found in August over the southwestern Tarim Basin, with the largest spatial extent, and to a lesser degree in September, where affected areas are markedly smaller.

3.3 Trend analysis of warm-season CBLH in Xinjiang at different temporal scales

Figure 5 presents the spatial distribution of the Sen's slope trends in the annual mean convective boundary layer height (CBLH) over Xinjiang during the warm season (April–September) at different temporal scales, based on the Mann–Kendall significance test. Only statistically significant trends at the $p < 0.05$ level are shown. At the 40-year scale (Figure 5a; 1985–2024), CBLH trends across most regions are relatively weak and spatially inconsistent. As the temporal scale decreases (Figure 5b; 2000–2024), a clearer pattern emerges: positive CBLH trends over the Tianshan Mountains become progressively stronger, while negative trends over the Tarim Basin intensify. However, when the temporal scale is further reduced (Figure 5c; 2015–2024), the magnitude of both the positive trends over the Tianshan Mountains and the negative trends over the Tarim Basin weakens.

3.4 Correlation analysis between warm-season CBLH and meteorological factors in key regions and months

As shown in Figure 6, for the Tianshan Mountains in July, the stepwise MLR retained eight significant predictors ($p < 0.01$) with $R^2 = 0.979$ (adjusted $R^2 = 0.978$), indicating high explanatory performance and reduced multicollinearity. The strongest positive effect on M_{blh} came from mountain skin temperature (M_{skt}, $+166.61$ m $^{\circ}\mathrm{C}^{-1}$), consistent with the role of local surface heating in enhancing convective mixing over complex terrain. Mountain zonal wind speed at 10 m [M_{u10}, $+18.11$ m $(\mathrm{m\ s}^{-1})^{-1}$] also contributed positively, possibly through enhanced mechanical turbulence.

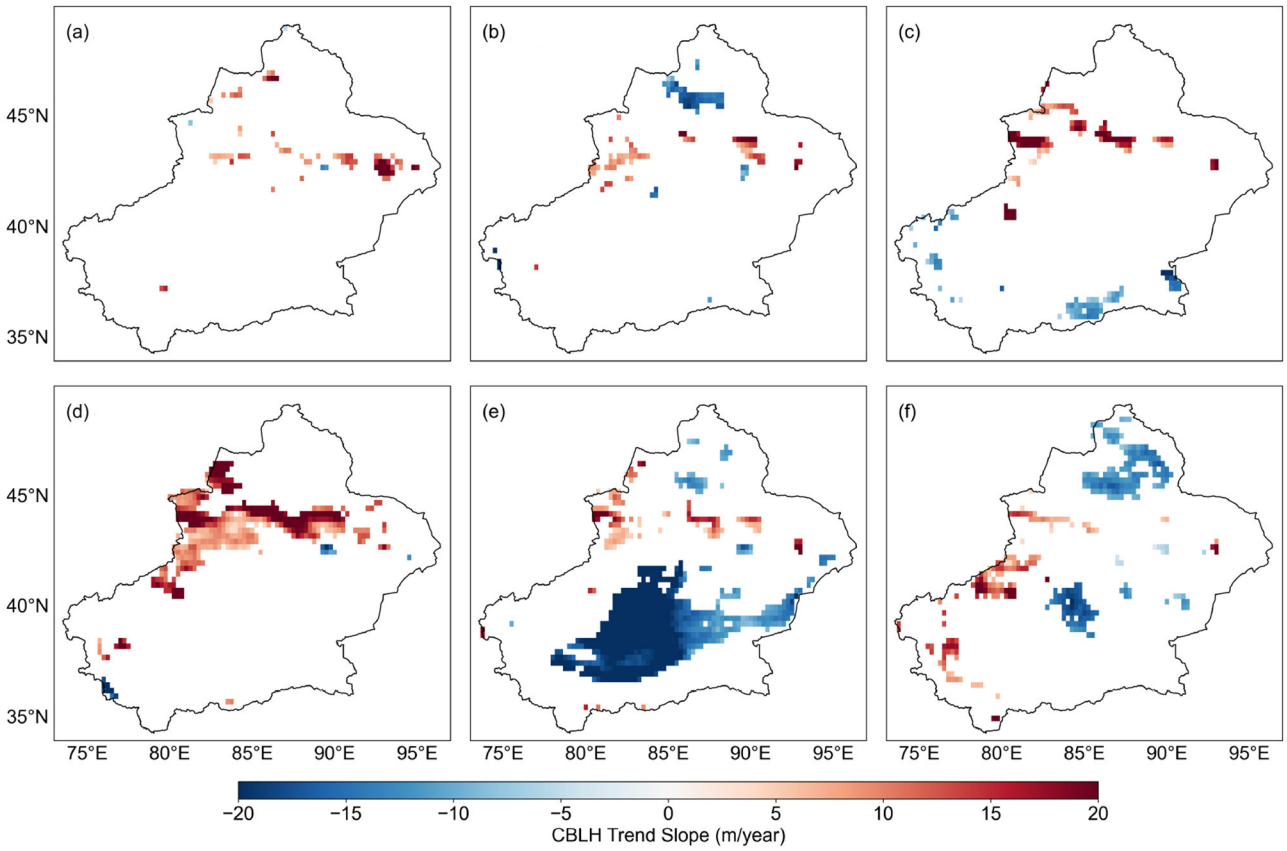

FIGURE 4
Spatial distribution of the monthly Sen's slope trends in convective boundary layer height (CBLH) over Xinjiang during the warm season (April–September) from 2000 to 2024. **(a–f)** Correspond to April through September. Only statistically significant trends ($p < 0.05$) are shown.

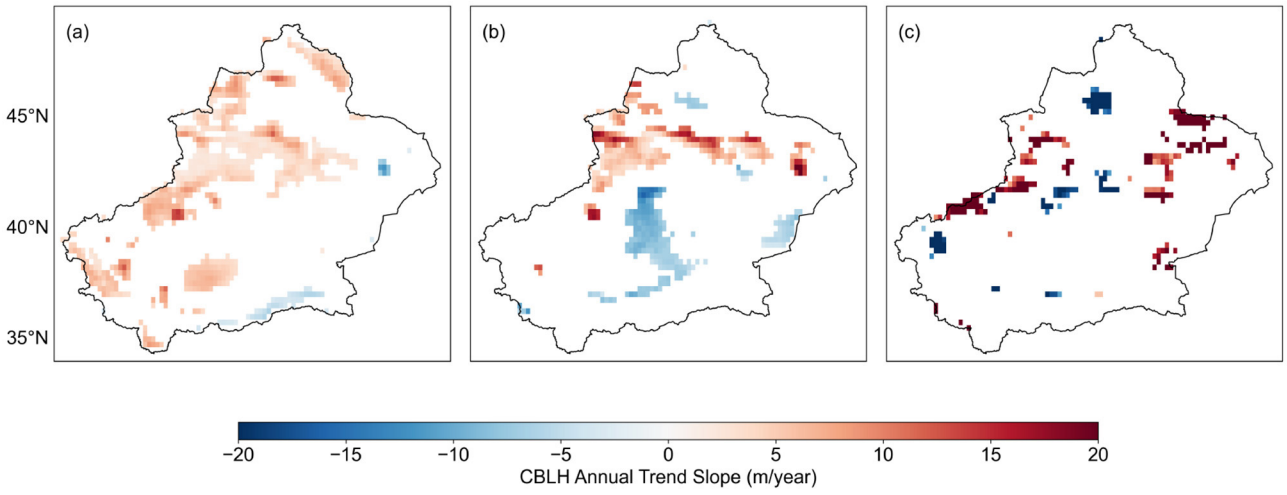

FIGURE 5
Spatial distribution of the annual mean CBLH trends over Xinjiang during the warm season (April–September) at different temporal scales, derived from the Sen's slope estimator after the Mann–Kendall significance test. Only statistically significant trends ($p < 0.05$) are shown. **(a–c)** Correspond to different time spans, with **(a)** 1985–2024, **(b)** 2000–2024, and **(c)** 2015–2024.

Negative predictors included mountain specific humidity [M_q, −138.31 m (kg kg^{-1})$^{-1}$], mountain surface sensible heat flux [M_{sshf}, −55.10 m (W m^{-2})$^{-1}$], and mountain surface net thermal radiation [M_{str}, −15.68 m (W m^{-2})$^{-1}$], implying that increased atmospheric moisture and altered radiative cooling tend to suppress CBLH growth. Signals from other subregions

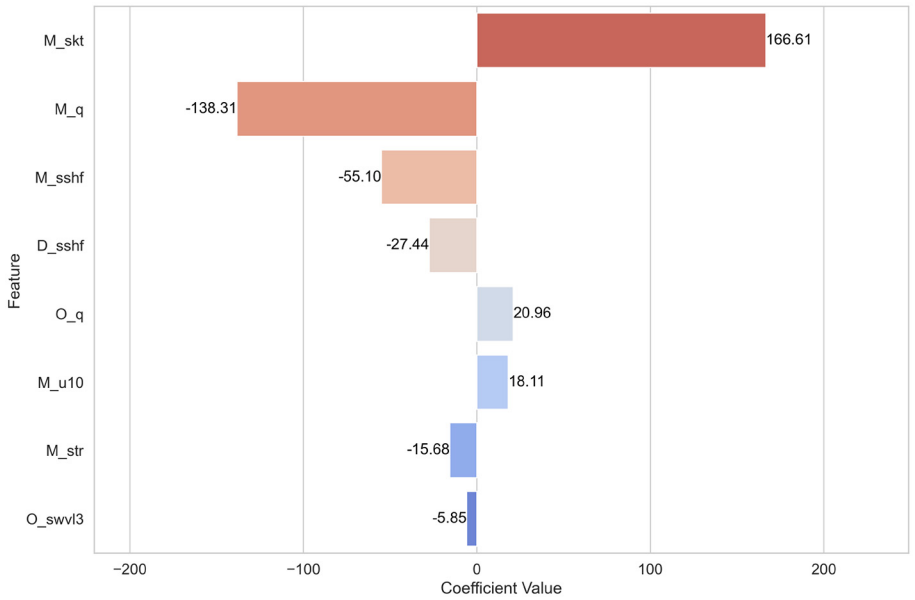

FIGURE 6
Regression coefficients of core predictors for the Tianshan Mountains' CBLH (M_{blh}) in July, based on the multiple linear regression model. Only statistically significant predictors ($p < 0.01$) are retained.

were also present: desert surface sensible heat flux [D_{sshf}, -27.44 m (W m^{-2})$^{-1}$] was negatively associated, while oasis specific humidity [O_q, $+20.96$ m (kg kg^{-1})$^{-1}$] and oasis deep-layer soil moisture [O_{swvl3}, -5.85 m (m^3 m^{-3})$^{-1}$] indicated cross-regional hydrothermal influences.

For the Taklamakan desert region in August, shown in Figure 7, the stepwise MLR model retained nine statistically significant predictors ($p < 0.01$), achieving high explanatory power ($R^2 = 0.955$, adjusted $R^2 = 0.951$) and substantially reducing multicollinearity relative to the full-variable model. The dominant positive predictor was desert skin temperature (D_{skt}, coefficient $+1011.88$ m °C^{-1}), underscoring the role of intense surface heating in deepening the CBLH. In contrast, oasis skin temperature (O_{skt}, -506.77 m °C^{-1}), oasis specific humidity [O_q, -294.22 m (kg kg^{-1})$^{-1}$], and oasis leaf area index (O_{LAI}, -63.72 m) exhibited significant negative associations, indicating that cooler, more humid, and vegetated conditions in oases suppress convective development via enhanced latent heat flux.

Radiative and thermal fluxes from the mountain region also influenced the desert CBLH negatively: surface net solar radiation [M_{ssr}, -392.30 m (W m^{-2})$^{-1}$], surface latent heat flux [M_{slhf}, -344.83 m (W m^{-2})$^{-1}$], and surface net thermal radiation [M_{str}, -128.03 m (W m^{-2})$^{-1}$]. These effects suggest that large-scale circulation and subsidence associated with mountain thermal conditions can modulate boundary layer development over the desert. Additionally, desert total cloud cover (D_{tcc}, $+115.92$ m) was positively correlated, possibly by reducing nocturnal longwave cooling. Deep-layer soil moisture [D_{swvl3}, -22.37 m (m^3 m^{-3})$^{-1}$] had a smaller but still significant negative effect.

Both models suggest the primary role of surface skin temperature in controlling warm-season CBLH, with positive effects in the local region of interest. However, moisture-related variables differ in their impact: in the desert region, higher specific humidity and vegetation cover suppress CBLH, while in the Tianshan Mountains, local humidity still has a negative effect, but oasis humidity shows a positive association. These factors indicate that anomalies in local and remote moisture, rather than direct cross-regional energy fluxes (which are not captured by upward/downward sensible heat flux or net radiation), contribute to the suppression of CBLH through altered atmospheric stability. The physical mechanisms inferred from these MLR results will be examined in greater detail in the subsequent PCA-based attribution analysis, to assess the consistency of statistical associations with the dominant modes of multivariate variability.

For July CBLH over the Tianshan region (M_{blh}, here M denotes Tianshan Mountain, O denotes oasis, and D denotes Taklamakan Desert), principal component analysis (PCA) of 39 meteorological and surface variables (Table 1) reveals that the first five principal components (PCs) account for 77.56% of the total variance, with PC1 and PC2 explaining 38.97% and 15.91%, respectively (Table 2). As shown in Figures 8a, b, PC1 exhibits a strong negative correlation with CBLH ($r = -0.67$) and primarily reflects variations in surface net longwave radiation ($O_{\mathrm{str}}, D_{\mathrm{str}}$), skin temperature ($O_{\mathrm{skt}}$), and surface sensible heat flux (O_{sshf}). PC2 is positively correlated with CBLH ($r = 0.67$) and is dominated by surface pressure ($O_{\mathrm{sp}}, D_{\mathrm{sp}}$) and mid-altitude skin temperature (M_{skt}). PCs 3–5 show weak correlations ($|r| < 0.12$) and smaller contributions.

For August D_{blh} over the Taklamakan Desert, PCA results show that the first five PCs explain 78.46% of the variance, with PC1 and PC2 accounting for 41.60% and 15.20%, respectively (Table 3, Figures 9a, b). PC1 has a strong negative correlation with D_{blh} ($r = -0.88$) and is mainly associated with net longwave radiation from both desert and oasis surfaces ($D_{\mathrm{str}}, O_{\mathrm{str}}$), oasis skin

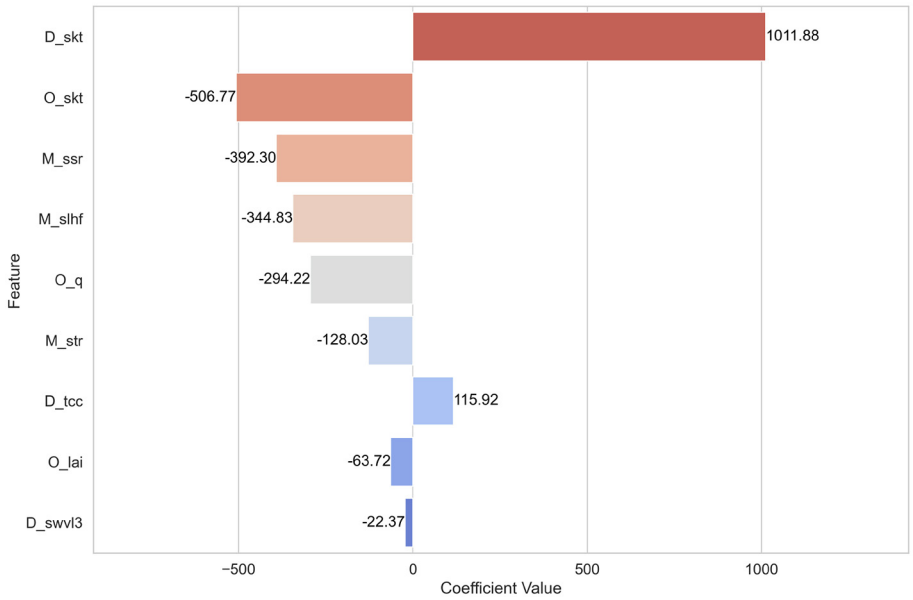

FIGURE 7
Regression coefficients of the core predictors for the desert region's convective boundary layer height (D_{blh}) in August, based on the multiple linear regression model. Only statistically significant predictors ($p < 0.01$) are retained in the model.

TABLE 2 PCA results for July M_{blh} in the Tianshan region: variance explained by the first five principal components (PCs), correlation coefficients (r) with M_{blh}, and top five contributing variables ranked by absolute loading values.

PC	Variance explained	r with M_{blh}	Top five contributing variables
PC1	0.39	−0.67	O_{str} (+0.24), O_{skt} (−0.24), D_{str} (+0.24), O_{sshf} (+0.24), D_{ssr} (—0.23)
PC2	0.16	+0.67	O_{sp} (+0.33), D_{sp} (+0.32), M_{skt} (+0.30), M_{sp} (+0.27), M_{str} (—0.26)
PC3	0.10	+0.12	O_{u10} (+0.36), D_{u10} (+0.35), M_{slhf} (+0.35), O_{swvl3} (+0.31), D_{swvl3} (+0.31)
PC4	0.07	+0.05	M_{u10} (+0.39), O_{tcc} (−0.26), M_{sp} (−0.25), D_{u10} (+0.24), O_{lai} (+0.23)
PC5	0.06	+0.02	D_{v10} (+0.41), O_{lai} (—0.34), M_{slhf} (−0.30), M_{swvl3} (+0.29), M_q (—0.25)

M denotes Tianshan Mountain, *O* denotes oasis, and *D* denotes the Taklamakan Desert.

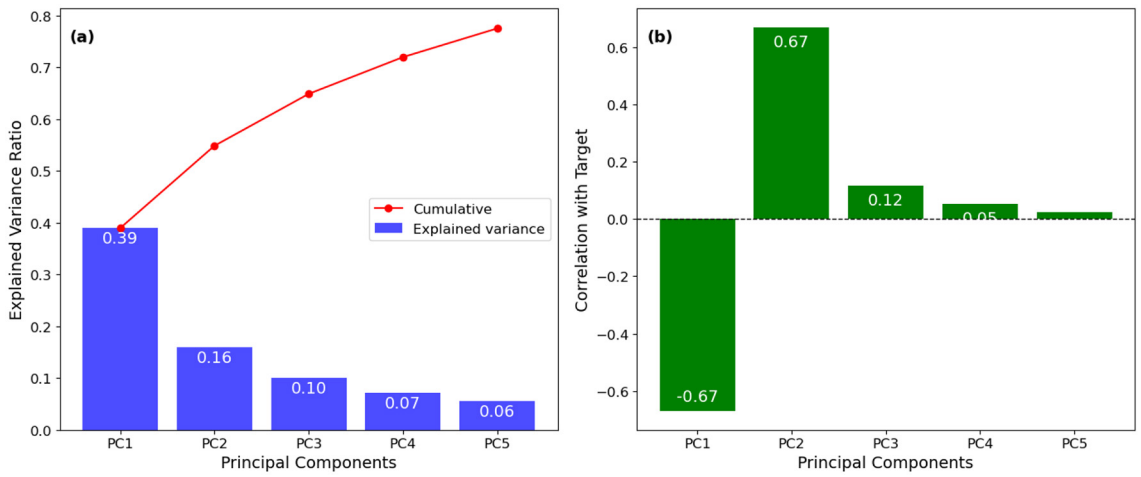

FIGURE 8
Principal component analysis results for July M_{blh} in the Tianshan region: **(a)** proportion of variance explained by each principal component (scree plot); **(b)** correlation between principal components and July M_{blh}.

temperature (O_{skt}), and surface net shortwave radiation (O_{ssr}, D_{ssr}). PC2 is weakly positively correlated ($r = 0.16$) and characterized by surface sensible heat flux (M_{sshf}), runoff (M_{ro}), deep-layer soil moisture (M_{swvl3}), oasis leaf area index (O_{LAI}), and mid-altitude net longwave radiation (M_{str}). PC5 ($r = -0.18$) underscores the role of mid-altitude skin temperature (M_{skt}), specific humidity (M_q), and deep-layer soil properties, while PCs 3 and 4 contribute little and have low correlations ($|r| < 0.14$). Overall, August D_{blh} variability is largely constrained by pronounced longwave cooling and reduced surface heating, with secondary modulation by sensible and latent heat exchange, soil moisture, and wind-related processes.

4 Discussion

The observed increase in July convective boundary layer height (CBLH) over the Tianshan Mountains may be linked to a combination of global warming-induced thermodynamic changes and regional topographic influences, based on statistical inferences from our analyses. Ongoing global warming may cause a general lifting of the troposphere, potentially facilitating a deeper convective boundary layer by reducing atmospheric stability and enhancing vertical mixing. This effect is most pronounced in July, the climatologically warmest month. Regions like the Tianshan Mountains may exhibit amplified warming due to their sensitivity to summer insolation and feedbacks from diminishing snow and glacier cover. Furthermore, the northern slopes of the Tianshan, acting as the windward side, may intercept warm and moist air masses advected from the north, leading to orographic forcing that could promote ascent, intensify convective instability, and thereby augment CBLH more substantially than on the southern slopes. These mechanisms appear to align with the principal component analysis (PCA) findings, where reduced net longwave cooling and enhanced sensible heating emerge as dominant modes; the former may arise from decreased atmospheric moisture or cloudiness that allows greater surface warming, while the latter could be fueled by increased solar absorption on exposed surfaces amid reduced albedo from melt. Lower surface pressure, another key PCA mode, likely stems from thermal lows induced by intense heating, potentially further destabilizing the boundary layer and promoting CBL growth.

The MLR and PCA analyses suggest why certain drivers may predominate in regulating CBLH variability across these subregions, as statistical associations. In the Tianshan during July, the primary positive influence of local skin temperature (M_{skt}) underscores the potential role of direct surface heating in driving buoyancy and entrainment, while negative effects from specific humidity (M_q) and sensible heat flux (M_{sshf}) may arise because excess moisture enhances radiative cooling and diverts energy to evaporation, dampening dry convection. Cross-regional signals, such as negative desert sensible heat flux (D_{sshf}) and positive oasis humidity (O_q), indicate mesoscale feedbacks whereby enhanced sensible heating over the desert intensifies low-level convergence and promotes compensating subsidence over adjacent mountain regions, reducing convective boundary layer growth through suppression of updrafts. In parallel, moisture originating from oasis evaporation and vegetation transpiration can be advected upwind, increasing near-surface relative humidity and enabling cold-air advection into arid zones. These processes enhance static stability, thereby inhibiting turbulent mixing and further modulating CBLH variability. For the desert in August, the dominance of oasis and mountain terms (e.g., negative M_{ssr}, M_{slhf}, M_{str}) suggests that radiative and latent fluxes from vegetated highlands may propagate downgradient, amplifying local humidity constraints and illustrating the interconnected hydrothermal dynamics of Xinjiang's heterogeneous landscape.

An additional layer of explanation involves large-scale atmospheric circulation influences, which modulate these local processes by altering moisture and energy transports. Xinjiang lies at the confluence of mid-latitude westerlies and the Asian summer monsoon (ASM) (Li et al., 2024), with interactions that exhibit anti-phase behavior on interannual to decadal scales under global warming. Strengthened westerlies, potentially linked to poleward shifts in jet streams amid Arctic amplification, enhance water vapor advection from the North Atlantic and Mediterranean into northwest China, increasing humidity in arid regions like the Taklamakan and suppressing CBLH through stabilized boundary layers (Zhao et al., 2022). Meanwhile, a weakened East Asian Summer Monsoon (EASM), driven by reduced land-sea thermal contrasts, allows greater westward penetration of westerly moisture, further humidifying the desert and contributing to the observed August declines. In the Tianshan, intensified westerlies amplify orographic lifting along northern slopes, boosting convective intensity and aligning with July increases. Teleconnections such as the negative phase of the Circumglobal Teleconnection/Silk Road Pattern (CGT/SRP), triggered by Indian Summer Monsoon heating anomalies, facilitate this by channeling Indian Ocean vapor northward via westerlies, while El Niño-Southern Oscillation (ENSO) events (e.g., La Niña) indirectly enhance westerly dominance by weakening the ASM (Sharma et al., 2024). These circulation dynamics, combined with local land surface changes, explain the divergent CBLH trends and highlight the need for integrated modeling of multi-scale interactions in future projections. Physically, cross-regional drivers manifest through mesoscale feedbacks: for instance, enhanced sensible heating over the Taklamakan Desert promotes low-level convergence, inducing compensating subsidence over the Tianshan Mountains that suppresses convective updrafts and reduces CBLH. In the oasis belt, vegetation-induced evapotranspiration fosters a cold-island effect, where cooler, moister air is advected into adjacent arid zones, increasing static stability (via reduced lapse rates) and inhibiting turbulent mixing.

Compared to prior investigations of boundary layer dynamics in arid and mountainous regions, this study provides a more comprehensive subregional analysis of warm-season CBLH trends and drivers across Xinjiang by integrating ERA5-Land reanalysis with GLASS LAI data and employing MLR alongside PCA to disentangle local, cross-regional, and large-scale influences. For example, while Salam et al. (2024) focused on planetary boundary layer height (PBLH, which includes but is not limited to CBLH) trends over the Tarim Basin using ERA5 data and identified overall declines linked to increased humidity from oasis expansion and irrigation, our work refines these findings by revealing monthly divergent patterns—such as July increases in the Tianshan versus August decreases in the Taklamakan—attributed to orographic

TABLE 3 PCA results for August D_{blh} in the Taklamakan Desert region: variance explained by the first five principal components (PCs), correlation coefficients (r) with D_{blh}, and top five contributing variables ranked by absolute loading values.

PC	Variance explained	r with D_{blh}	Top five contributing variables
PC1	0.41	−0.88	D_{str} (+0.24), O_{str} (+0.23), O_{skt} (−0.23), O_{ssr} (−0.23), D_q (+0.22)
PC2	0.16	+0.19	M_{sshf} (+0.31), M_{blh} (−0.29), M_{ro} (+0.28), M_{swvl3} (+0.27), O_{LAI} (-0.26)
PC3	0.09	−0.14	M_{slhf} (+0.39), O_{swvl3} (+0.34), M_{tcc} (+0.33), D_{swvl3} (+0.30), M_{skt} (-0.23)
PC4	0.07	+0.10	M_{u10} (+0.31), M_{sp} (−0.30), O_{u10} (+0.28), M_{ssr} (+0.26), O_{ro} (+0.25)
PC5	0.05	−0.18	M_{skt} (+0.41), M_q (+0.39), O_{swvl3} (+0.37), D_{swvl3} (+0.28), O_q (+0.25)

M denotes Tianshan Mountain, *O* denotes oasis, and *D* denotes the Taklamakan Desert.

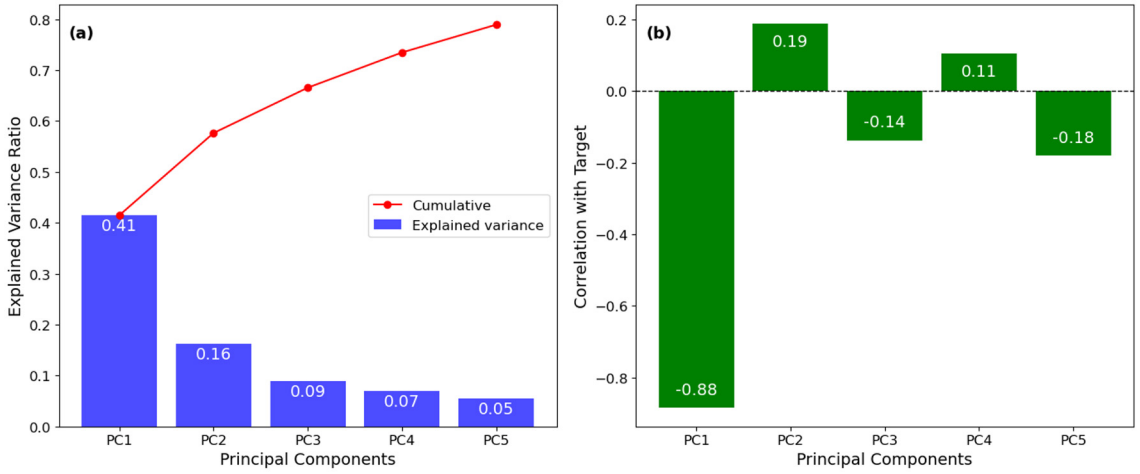

FIGURE 9
Principal component analysis results for August D_{blh} in the Taklamakan desert region: **(a)** proportion of variance explained by each principal component (scree plot); **(b)** correlation between principal components and D_{blh}.

and cryospheric feedbacks, with PCA highlighting distinct modes of radiative and moisture variability not emphasized in their basin-centric approach. Similarly, Zhao et al. (2022) examined summer ABLH relationships with land surface parameters and Eurasian circulations in the Taklamakan Desert, noting positive correlations with sensible heat flux and negative with soil moisture, but our analysis extends this by quantifying cross-subregional interactions (e.g., oasis humidity suppressing desert CBLH) and incorporating teleconnections like the CGT/SRP, offering a multi-scale perspective absent in their localized study. On a broader scale, Man et al. (2021) compared long-term PBLH trends across China using observations and CMIP6 models, finding general increases driven by warming but with regional variations; however, our Xinjiang-specific focus uncovers unique arid-mountain contrasts and ecological interventions that may be diluted in national aggregates, underscoring the value of high-resolution datasets for complex terrains. These distinctions highlight how the integrated methodology employed in this study advances understanding of CBLH evolution in mid-latitude arid environments, particularly under compounded climate and land-use changes.

Although this study applies robust statistical approaches (MLR, PCA) to explore the drivers of CBLH variability, these methods primarily reveal associations and cannot definitively establish causality. Some of the inferred mechanisms, while supported by statistical trends and existing physical theory, require further validation through process-based modeling and observational experiments.

5 Conclusions

1. Xinjiang's warm-season (April–September) CBLH exhibits clear spatial organization, with basins showing higher values than mountains and a seasonal peak in June–July.
2. Over 2000–2024, the Tianshan experienced significant July CBLH increases, while the Taklamakan Desert saw notable August declines.
3. Stepwise MLR analysis identified D_{skt} as the dominant positive driver for August CBLH in the desert, with strong negative controls from O_{skt}, O_q, and O_{LAI}, and additional suppression from mountain-region radiative and latent heat fluxes. In the Tianshan during July, M_{skt} was the primary positive driver, while M_q, M_{sshf}, and D_{sshf} exerted significant negative effects.
4. PCA further clarified the dominant physical modes: radiation balance, sensible heating, and surface pressure in the Tianshan; enhanced longwave cooling, reduced net heating, and increased humidity in the desert.

5. Regional climate projections should account for the concurrent but opposing influences that the coexistence of warming-driven CBLH increases and moisture-driven declines in neighboring subregions, as well as the cross-regional transfer of thermal and moisture signals.

These results highlight the complexity of land-atmosphere interactions in arid, topographically diverse mid-latitude environments, and suggest the value of combining MLR and PCA to disentangle local and remote controls on CBLH variability. Such integrated approaches can support tailored adaptation strategies under future climate change scenarios.

Data availability statement

The original contributions presented in the study are included in the article/supplementary material, further inquiries can be directed to the corresponding author.

Author contributions

HS: Conceptualization, Writing – original draft, Writing – review & editing. YL: Formal analysis, Writing – original draft. CL: Conceptualization, Writing – original draft. SW: Validation, Writing – original draft. ZW: Data curation, Visualization, Writing – original draft. WG: Resources, Writing – review & editing. JW: Investigation, Writing – review & editing.

Funding

The author(s) declare that no financial support was received for the research and/or publication of this article.

Conflict of interest

The authors declare that the research was conducted in the absence of any commercial or financial relationships that could be construed as a potential conflict of interest.

Generative AI statement

The author(s) declare that no Gen AI was used in the creation of this manuscript.

Any alternative text (alt text) provided alongside figures in this article has been generated by Frontiers with the support of artificial intelligence and reasonable efforts have been made to ensure accuracy, including review by the authors wherever possible. If you identify any issues, please contact us.

Publisher's note

References

Bhattacharya, A., Bolch, T., Mukherjee, K., King, O., Menounos, B., Kapitsa, V., et al. (2021). High mountain Asian glacier response to climate revealed by multi-temporal satellite observations since the 1960s. *Nat. Commun.* 12:4133. doi: 10.1038/s41467-021-24180-y

Brunsell, N. A., Mechem, D. B., and Anderson, M. C. (2011). Surface heterogeneity impacts on boundary layer dynamics via energy balance partitioning. *Atmos. Chem. Phys.* 11, 3403–3416. doi: 10.5194/acp-11-3403-2011

He, B., Sheng, Y., Cao, W., and Wu, J. (2020). Characteristics of climate change in northern Xinjiang in 1961–2017, China. *Chin. Geogr. Sci.* 30, 249–265. doi: 10.1007/s11769-020-1104-5

He, X., Zhang, L., Lu, Y., and Chai, L. (2024). Spatiotemporal variations of vegetation and its response to climate change and human activities in arid areas–a case study of the Shule River Basin, Northwestern China. *Forests* 15:1147. doi: 10.3390/f15071147

Hersbach, H., Bell, B., Berrisford, P., Hirahara, S., Hornyi, A., Muoz-Sabater, J., et al. (2020). The era5 global reanalysis. *Q. J. R. Meteorol. Soc.* 146, 1999–2049. doi: 10.1002/qj.3803

Jolliffe, I. T. (2002). *Principal Component Analysis*, 2nd Edn. New York, NY: Springer.

Kendall, M. G. (1975). *Rank Correlation Methods*, 4th Edn. London: Charles Griffin.

Li, M., Zhang, Z., Ju, C., and Li, H. (2023). Sensitivity of temperature and precipitation characteristics to land use classification over the Taklimakan Desert and surrounding area. *Theor. Appl. Climatol.*154, 987–998. doi: 10.1007/s00704-023-04608-9

Li, X., Huang, A., Zhao, Y., Feng, T., Wang, S., Yang, F., et al. (2024). Interaction between the westerlies and Asian monsoons in the middle latitudes of China: review and prospect. *Atmosphere* 15:274. doi: 10.3390/atmos15030274

Lieman, R., and Alpert, P. (1993). Investigation of the planetary boundary layer height variations over complex terrain. *Boundary - Layer Meteorol.* 62, 129–142. doi: 10.1007/BF00705550

Lu, Y., Yu, Y., Sun, L., Li, C., He, J., Guo, Z., et al. (2025). NDVI based vegetation dynamics and responses to climate change and human activities at Xinjiang from 2001 to 2020. *Sci. Rep.* 15:25848. doi: 10.1038/s41598-025-11677-5

Ma, H., and Liang, S. (2022). Development of the glass 250-m leaf area index product (version 6) from modis data using the bidirectional LSTM deep learning model. *Remote Sens. Environ.* 273:112985. doi: 10.1016/j.rse.2022.112985

Man, Y., Wang, M., Guo, J., Zhang, H., Dong, X., Liu, Y., et al. (2021). Long-term trend comparison of planetary boundary layer height in observations and cmip6 models over China. *J. Clim.* 34, 8237–8256. doi: 10.1175/JCLI-D-20-1000.1

Mann, H. B. (1945). Nonparametric tests against trend. *Econometrica* 13, 245–259. doi: 10.2307/1907187

Muñoz Sabater, J., Dutra, E., Agustí-Panareda, A., Albergel, C., Arduini, G., Balsamo, G., et al. (2021). Era5-land: a state-of-the-art global reanalysis dataset for land applications. *Earth Syst. Sci. Data* 13, 4349–4383. doi: 10.5194/essd-13-4349-2021

Salam, A., He, Q., Abbas, A., Wu, T., Zhang, J., Jie, W., et al. (2024). Boundary layer height and trends over the tarim basin. *Atmosphere* 15:541. doi: 10.3390/atmos15050541

Sen, P. K. (1968). Estimates of the regression coefficient based on Kendall's tau. *J. Am. Stat. Assoc.* 63, 1379–1389. doi: 10.1080/01621459.1968.10480934

Sharma, A. R., Dimri, A. P., and Tiwari, S. (2024). The impact of the summer monsoon on the convective boundary layer height in different regions of the Tibetan plateau. *Atmos. Res.* 299:107213. doi: 10.1016/j.atmosres.2024.107252

Stull, R. B. (1988). *An Introduction to Boundary Layer Meteorology*. Dordrecht: Springer Netherlands. doi: 10.1007/978-94-009-3027-8

Theil, H. (1950). A rank-invariant method of linear and polynomial regression analysis. *Nederl. Akad. Wetensch. Proc*. 53, 386–392.

Wang, M., and Zhang, J. (2022). The relationship among summer atmospheric boundary layer height over the Taklimakan Desert, its land surface parameters and Eurasian circulation. *Atmos. Sci. Lett*. 23:e1122. doi: 10.1002/asl.1122

Wang, Y., Sayit, H., Mamtimin, A., Zhu, J., Zhou, C., Huo, W., et al. (2021). Evaluation of five planetary boundary layer schemes in WRF over China's largest semi-fixed desert. *Atmos. Res*. 256:105567. doi: 10.1016/j.atmosres.2021.105567

Wang, Y., Xu, T., Shi, G., Yang, F., Tang, X., Zhao, X., et al. (2023). Climatology of the planetary boundary layer height over China and its characteristics during periods of extremely temperature. *Atmos. Res*. 294:106960. doi: 10.1016/j.atmosres.2023.106960

Wu, W., Chen, H., Guo, J., Xu, Z., and Zhang, X. (2024). Regionalization of the boundary-layer height and its dominant influence factors in summer over China. *Chin. J. Atmos. Sci*. 48, 1201–1216. doi: 10.3878/j.issn.1006-9895.2212.22183

Xiao, Z., Liang, S., Wang, J., Xiang, Y., Zhao, X., Song, J., et al. (2016). Long-time-series global land surface satellite leaf area index product derived from MODIS and AVHRR surface reflectance. *IEEE Trans. Geosci. Remote Sens*. 54, 5301–5318. doi: 10.1109/TGRS.2016.2560522

Zardi, D. (2007). On the boundary-layer structure over highly complex terrain: key findings from map. *Q. J. R. Meteorol. Soc*. 133, 937–948. doi: 10.1002/qj.71

Zhang, K., Dai, S., and Dong, X. (2020). Dynamic variability in daily temperature extremes and their relationships with large-scale atmospheric circulation during 1960–2015 in xinjiang, China. *Chin. Geogr. Sci*. 30, 233–248. doi: 10.1007/s11769-020-1106-3

Zhang, X., Cai, C., Hu, X.-M., Gao, L., Xu, X., Hu, J., et al. (2022). Aerosols consistently suppress the convective boundary layer development. *Atmos. Res*. 269:106032. doi: 10.1016/j.atmosres.2022.106032

Zhao, Y., Huang, A., Yang, F., Feng, T., and Wang, S. (2022). The relationship among summer atmospheric boundary layer height in the Taklamakan desert, land surface parameters and large-scale circulations. *Atmos. Sci. Lett*. 23:e1122.